Interplay between Energy-Level Position and Charging Effect of Manganese Phthalocyanines on an Atomically Thin Insulator

Liwei Liu, Thomas Dienel, Roland Widmer, and Oliver Gröning*

Empa, Swiss Federal Laboratories for Materials Science and Technology, Überlandstrasse 129, CH-8600 Dübendorf, Switzerland

ABSTRACT Understanding the energy-level alignment and charge transfer of organic molecules at large bandgap semiconductors is of crucial importance to optimize device performance in organic electronics. We have studied submonolayer coverage of manganese phthalocyanine (MnPc) on hexagonal boron nitride (h-BN) on Rh(111) as a model system by low-temperature scanning tunneling microscopy (STM) and spectroscopy (STS). The adsorbed molecules show three distinctly different bias-dependent topographic signatures, which depend on their adsorption positions on the h-BN. Among these three types of MnPc, one shows pronounced charging because of the proximity of the highest occupied molecular orbital (HOMO) to the Fermi level on the decoupling h-BN substrate. The charging of the MnPc from its neutral to the $MnPc^+$ state leads to a down shift of the Mn 3*d*-related orbital by 840 meV as determined from the difference in energy position between high- and low-bias charging. We find that the charging field is linearly related to the HOMO position with respect to the Fermi level, with a clear correlation to the adsorption orientations of the MnPc. Our results show how critically energy level alignment and field-induced charge transfer process can depend on adsorption configurations, even on an apparently low-interacting substrate like metal supported monolayer h-BN.

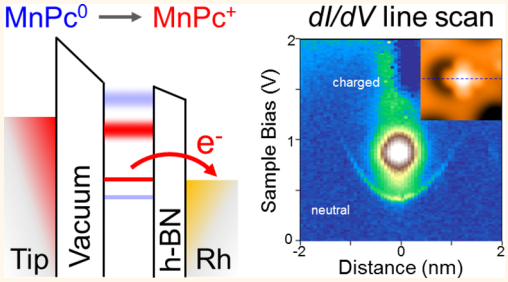

KEYWORDS: hexagonal boron nitride · molecular adsorption · charging effect · molecular orbital · scanning tunneling microscopy · scanning tunneling spectroscopy

Applications of organic materials in electronics and catalysis are strongly dependent on charge transfer processes at immanent organic−inorganic interfaces. In recent years, particular attention has been devoted to the interface between molecular materials and large bandgap semiconductors in view of their application in dye-sensitized solar cells, organic light-emitting diodes, and photocatalysis, where transition metal oxides serve as electrode materials.[1−4] An optimization of the charge carrier injection is directly related with tuning the charge transfer barriers, which requires a detailed understanding of the alignment of the molecular orbitals (mainly the highest occupied molecular orbital (HOMO) and lowest unoccupied molecular orbital (LUMO)) with the valence and conduction band of the semiconductor.[5] However, most studies of molecular adsorption rely on metallic substrates, where the molecular orbitals might be altered by hybridization with the valence electrons of the metal.[6−9] Thus, ultrathin, large bandgap materials grown on metal surfaces (like NaCl, CuN and Al_2O_3)[10−13] have been praised as ideal substrates, as their insulating nature preserves the intrinsic electronic structure of adsorbates, while permitting scanning tunneling microscopy (STM) to study the atomic structure and electronic properties of the adsorbate. In this respect, single layer hexagonal boron nitride (h-BN) grown on metal surfaces[14−24] has been attracting increasing interest as substrate, due to its simple, self-limited growth and various superstructures that form depending on the choice of the metal support. In this paper, we have used manganese phthalocyanine (MnPc) adsorbed on a single layer of h-BN on Rh(111) as a model system to investigate the interplay between energy level alignment and field-induced charge transfer at the single molecular level.

Recently, metal phthalocyanine and free-base porphine molecules on h-BN grown on

* Address correspondence to oliver.groening@empa.ch.

Received for review June 19, 2015 and accepted September 21, 2015.

Published online September 21, 2015
10.1021/acsnano.5b03741

metal surfaces have been studied,[21,22,24] where STM results revealed high resolution molecular orbitals and corresponding narrow peaks in the d*I*/d*V* spectra, indicating low electronic hybridization between the molecules and the substrate. Importantly, depending on the adsorption site, a rigid energy shift of the molecular orbitals due to work function changes within the unit cell of the h-BN/metal moiré[22] or a reordering of the molecular orbitals due to charging could be observed.[21,24]

As field-induced charge transfer involves a shift of the molecular orbitals[25] or the conduction band,[26,27] it always manifests as a sharp peak in the d*I*/d*V* spectra, similar to a density of states (DOS) feature of decoupled molecules. Thus, it is necessary to discriminate between the charging peak and the molecular DOS within the same energy range to understand their relation and interplay. Here, we observe a shift of the molecular orbital, resulting in a sudden enhancement of the tunneling current. Spatial-dependent d*I*/d*V* mapping allows to clearly identify the Mn 3*d* related orbital, the charging peak and how this *d* orbital is influenced by the "low bias" and "high bias" charging effect. Two orientations of molecules with a small energy shift of the HOMO can strongly change the charging bias and therefore switch the ability of the molecule to be charged.

RESULTS AND DISCUSSION

Figure 1a shows a large scale STM topography image at 4.9 K of a monolayer of h-BN on Rh(111) covered with MnPc molecules (equivalent to 15% of a densely packed monolayer). The h-BN surface forms a hexagonal superstructure of 3.2 nm periodicity, which arises from the 7% lattice mismatch between h-BN and Rh(111).[14] Topographic depression and protrusion regions are called pore and wire regions and differ from each other by the interaction of the h-BN with the Rh(111) substrate.[28] As other molecular or atomic species, the MnPc selectively adsorbs in the pore regions of the h-BN/Rh(111) with a systematic off-center position at low coverage.[14,18,19,23] Although all molecules are trapped at similar positions with respect to the superstructure of the h-BN/Rh(111), three different STM topographic signatures of the MnPc can be identified. Examples of these three signatures are shown in Figure 1b taken at 0.2 V STM bias. The three types, highlighted by colored circles, are characterized by (i) a cross like appearance with a dark center (DC, yellow circle), (ii) a similar cross like structure but with a bright center (BC, blue circle), and (iii) a D_{2h} symmetry structure exhibiting one and two lobes, respectively, at the neighboring isoindole moieties (six-lobe, red circle). The differences in the STM appearances are not limited to imaging at 0.2 V bias, but extend throughout the bias window from −2 V to +2 V (*cf.* Supporting Information paragraph 1). Outside this bias window we detect strong contributions from the substrate, which mask the intrinsic features of the molecules.

In order to verify the identical chemical nature of the three different types and to exclude the presence of impurity species, *e.g.*, metal-free phthalocyanine (H_2Pc), we performed STM tip-induced manipulation[29] and monitored the changes in appearance of the molecules. Each of the three different types can be reversibly changed into the others, as exemplified in Supporting Information Figure S2, suggesting their identical chemical structure. Topographic effects due to gas molecule decoration, well-known for MnPc molecules,[30−32] could be excluded by the use of voltage pulses (3 V with a STM loop bias of 0.2 V at 1 nA), where no change is observed, as long as the position of the MnPc molecule remains the same. Consequently, the different STM signatures seem to originate from

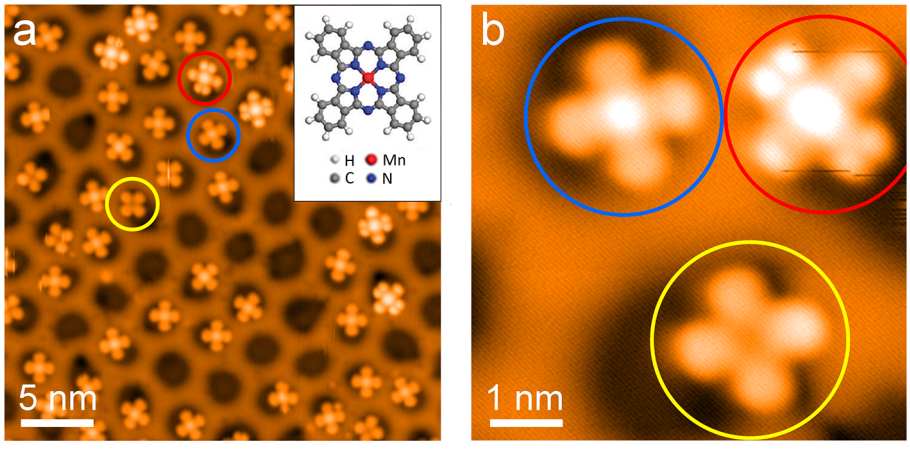

Figure 1. STM topographic signatures of MnPc molecules on the h-BN/Rh(111). (a) STM image (0.2 V, 20 pA) of the MnPc adsorption within the pores of the h-BN/Rh(111) (regular network of depressions). Three different topographic types of the MnPc can be distinguished. Inset: molecular structure of MnPc. (b) High-resolution STM image of neighboring pores hosting single MnPc molecules with different signatures, denoted as bright center (BC), dark center (DC) and six-lobe MnPc (as indicated by blue, yellow, and red circle, respectively).

subtle differences of the adsorption site of the individual MnPc molecules (*cf.* Supporting Information: Structural integrity and purity of the adsorbed MnPc), influencing their conformational or electronic state.[33]

Statistical evaluation of the occurrence of the three types of MnPc on the h-BN/Rh(111) shows that BC MnPc is the most frequent one (70%), while the other two types (DC and six-lobe) occur with nearly equal abundance (15%; *cf.* Supporting Information Figure S4). Although the atomic details of the different appearances are not fully clear at the moment for all the three types, we have a good understanding of the behavior of the BC MnPc. As we will discuss in the following, the BC MnPc molecules exhibit between themselves varying characteristics, which can be understood from differences in field-induced charge transfer.

The spectroscopic characterization of the BC MnPc on the h-BN/Rh(111) is summarized in Figure 2. The d*I*/d*V* spectra reveal the variability in peak positions and intensity at positive bias from one molecule to another (*cf.* center M1, M2, and M3 in Figure 2a). Additional features close to the Fermi energy are observed in the spectrum taken at the isoindole unit of the MnPc molecule (Lobe M1). The sequence of peaks in the bias range from −0.5 to 0 V, can be attributed to the HOMO. The contribution of the HOMO leads to a drastic contrast change in the STM topography, when the bias is changed from +0.2 V to −0.15 V (*cf.* Gap and HOMO in Figure 2b, respectively; biases are indicated by colored arrows in Figure 2a). The d*I*/d*V* spectrum taken at the center of the same molecule (*cf.* Center M1 in Figure 2a) shows a markedly different signature: the HOMO is not visible anymore, the sharp peak is shifted down by 100 meV from +0.73 V (Lobe) to +0.63 V, and a new feature occurs in the form of a very intense broad peak centered at +0.92 V. It is interesting to note that the positions of these two features at positive bias can vary dramatically between different BC MnPc molecules. The spectrum Center M2 in Figure 2a, measured on a different BC MnPc, shows a sharp peak at about +1.8 V and a broad peak at +1.6 V, now preceding the sharp peak. Finally, the spectrum taken at Center M3, measured on a further BC MnPc, shows no sharp peak and the broad peak is at the same position as in the case of molecule M2.

Before we turn to the explanation of this variability, we focus our attention to the fine structure of the HOMO. If the set point parameters for the d*I*/d*V* are appropriately chosen (*e.g.*, −0.1 V, 100 pA, to bring the tip closer to the molecule), the HOMO feature can also be observed at the center of the molecule as seen from Figure 2c, revealing a vibronic multiplet of equally spaced peaks.[34] Typically, these vibronic peaks[21,35,36] are observed for decoupled molecular orbitals, where the lifetime of a given electronic state is long enough to enable an electron (tunneling to this state) to couple to vibrational modes. As shown in Figure 2c,

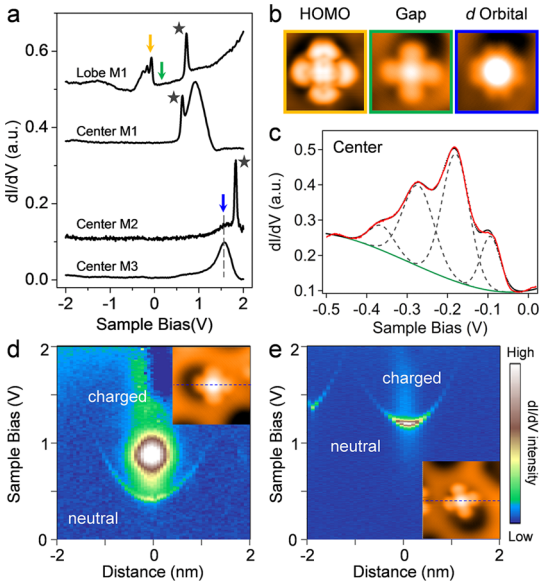

Figure 2. Electronic characterization of BC MnPc molecules on the h-BN/Rh(111). (a) d*I*/d*V* spectra of BC MnPc molecules, showing vibronic peaks at the molecular lobe in the HOMO position (Lobe M1), and three kinds of spectra with different peak positions at the molecular centers (labeled as Center M1, M2 and M3). The sharp peaks are marked by the asterisks. STM settings before opening feedback (FB) loop: 2 V, 200 pA. (b) STM topographies scanned at several typical biases marked by the arrows in (a), showing the molecular orbitals (images with yellow and blue frame) and the conductance gap (the image with a green frame). Scanning parameters are −0.15, 0.2, and 1.6 V (from left to right) at 20 pA; image size: 2.5 nm × 2.5 nm. (c) The vibronic substructure of the HOMO at the molecular center (black curve) can be fitted with a sum (red curve) of four Gaussians (dashed gray curves). STM settings before opening FB loop: 0.1 V, 100 pA. (d) Equidistant d*I*/d*V* spectra taken at constant height (open loop) across a BC MnPc along the dashed line in inset (0.2 V, 20 pA, size: 4 nm × 4 nm). The pronounced bright "arc" ranging from 0.4 to 2 V indicates the "low bias" charging, whereas the intense maximum at the molecular center at 0.8 V originates from the Mn 3d orbital. STS settings before opening FB loop: 1 V, 500 pA at MnPc center. (e) Equidistant d*I*/d*V* spectra taken at constant height (open loop) along the dashed line in inset (0.2 V, 20 pA, size: 4 nm × 4 nm). The sharp bright "arc" ranging from 1.3 to 2 V belongs to "medium bias" charging. STS settings before opening FB loop: 2 V, 200 pA at MnPc center.

these peaks can be very well fitted by a sum of four Gaussians on a cubic background. We consistently find that in the molecule center the first phonon excitation peak is strongest as opposed to the lobe position, where the elastic peak is dominant (*cf.* Supporting Information Figure S5). A linear regression fitting of the peak positions against the peak number yields an estimate of the energy of the vibrational mode of V_{vib} = 97 ± 5 meV. The accurate determination of the vibrational mode energy requires a correction due to the voltage drop at the h-BN ultrathin insulator, to which the double barrier tunneling junction (DBTJ) model can be applied.[25,37,38] The actual energy spacing should be rescaled to $(V_{vib})_{corr} = (1 - \alpha)V_{vib}$, with the fraction of the voltage drop over the molecule α = 0.093 (will be discussed in detail later), yielding 88 meV

(corresponding to 710 cm^{-1}). Possible candidates for this vibration are the out of plane B_{2g} mode (700 cm^{-1}) or the red-shifted E_{1g} mode (838 cm^{-1}) of benzene.[39,40]

In order to clarify the nature of the spectroscopic features in the positive bias range of the BC MnPc, we have measured d*I*/d*V* maps across the molecules, *i.e.*, d*I*/d*V* spectra as a function of tip position. Two such STS maps are shown in Figures 2d,e (see insets for topography of the corresponding molecule; dashed line denotes the path of the STM tip). A distinct parabolic-like feature can be discerned in both maps, which has its bias minimum and intensity maximum at the center of the molecule. This feature corresponds to the sharp peak highlighted by the asterisks throughout the spectra in Figure 2a. Its strong dispersion in energy as a function of tip position implies that it is not a DOS feature. Rather it denotes a sudden change of the charge state of the molecule, depending on the bias and the tip position, *i.e.*, the applied electric field. Similar phenomena have been observed for impurity ions in organics,[25,38,41,42] semiconducting layers,[26,27,43] and adatoms on graphene[44] and have been attributed to field assisted charging. The charging process is reversible without hysteresis, as d*I*/d*V* spectra measured with forward (from low to high bias) and backward ramp direction are essentially identical.

The charging separates each spectrum and each STS map into two parts: Below the charging peak (scan with lower bias than the charging bias) the molecule is measured in its neutral state $MnPc^0$ and above the charging peak (scan with higher bias than the charging bias) in the charged state $MnPc^+$. Depending on the bias when the charging occurs at the position of the molecule center, we differentiate the cases as "low bias" charging and "high bias" charging (*cf.* molecules M1 and M2 in Figure 2a, respectively). In the case of sample molecule M3, the charging does not occur below 2 V but presumably belongs to the class of "high bias" charging. The charging peak can also be observed in the bias range from 0.9 to 1.7 V without the appearance of the broad peak, which we denote as "medium bias" charging. Figure 2d shows a "low bias" charging case, while a "medium bias" charging example is shown in Figure 2e. We attribute the broad feature located at the center of the molecule to a 3*d*-related orbital of the Mn atom (*cf.* corresponding topographic STM signature in Figure 2b). For the "medium bias" charging case only a faint front and tail before and after the charging peak is observed, instead of a broad peak. The relative d*I*/d*V* intensity varies between "low bias" charging and "medium bias" charging, while the first shows the highest intensity at the *d* orbital, the latter shows the highest at the charging peak (*cf.* corresponding *I*(*V*) curves in Supporting Information Figure S6).

In addition to the spectral dependence on the lateral tip position shown in the d*I*/d*V* maps in Figures 2d,e, we have also investigated the dependence on the vertical tip position and studied the evolution of the three charging cases. The top curve in Figure 3a shows a "low bias" charging effect at a set point of 400 pA.

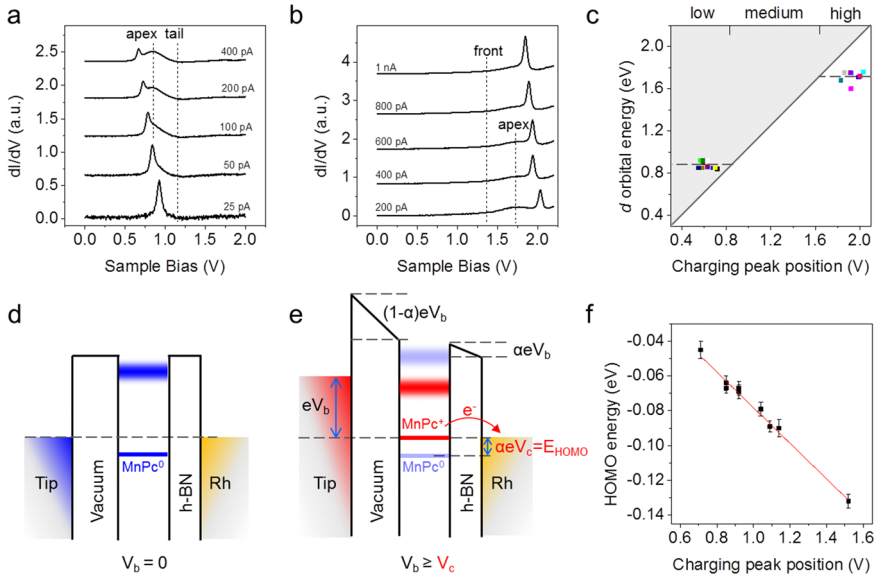

Figure 3. Interplay between charging peak, d orbital and HOMO of BC MnPc. (a,b) d*I*/d*V* spectra at the center of BC MnPc molecules, measured at different current set points for "low bias" (a) and "high bias" (b) charging. The charging peaks show a pronounced shift, while the tail or front of the d orbital remains basically unchanged (indicated by dotted vertical lines). Note that the spectra are rescaled to the same current set point, *e.g.*, intensity of the curve taken at 100 pA is multiplied by 4 for easy comparison to that taken at 400 pA (STM bias before FB loop is open: 2 V). (c) Statistical analysis of the relation between the energetic position of the chargingpeak and the 3d orbital (analysis of d*I*/d*V* spectra at 44 individual BC MnPc molecules, taken at 2 V, 200 pA before opening FB loop). The energy ranges to differentiate the charging cases are marked at the top of the graph. (d,e) Schematics of the positive charging process, showing the down shift of the 3d-related orbital, when charging occurs. (f) Relation between charging peak position and energy of HOMO at the molecular center.[45]

With a decrease in set point, *i.e.*, the tip moves farther away from the molecule, the position of the sharp charging peak shifts from +0.67 V toward higher bias, indicating its dependence on the electric field (for the direct relationship between tip height and position of the charging peak see Supporting Information Figure S8). By contrast, the *d* orbital peak at higher energies remains at a fixed position of ~ +0.8 V, unaffected by the change in set point parameters. Below a set point current of 50 pA the charging peak is up-shifted beyond the apex of *d* orbital peak rendering the latter invisible. In the "high bias" charging regime (*cf.* Figure 3b) a similar upshift of the charging peak is observed when decreasing the current set point, but the *d* orbital peak appears at lower energy than the charging peak and remains at a fixed position of ~ +1.7 V. Figure 3c summarizes the *d* orbital energies for a number of different BC MnPc molecules as a function of charging peak position (analysis of d*I*/d*V* spectra all measured with 2 V, 200 pA before opening FB loop). Two groups of points can be clearly distinguished: Group one, where the charging peak is below the position of the *d* orbital peak. In this case the *d* orbital position is assigned to $MnPc^+$ at 0.87 ± 0.03 V, whereas for group two the charging peak is above the *d* orbital peak position of 1.71 ± 0.05 V, which belongs to the neutral $MnPc^0$. In the "medium bias" charging case (between 0.87 and 1.71 V), the position of the *d* orbital cannot be determined due to its jump in energetic position upon charging the MnPc molecule.

The remaining question is on the origin of the large variation of the charging voltage or more precisely the charging field among different BC MnPc molecules. To answer this question, the charging process is illustrated in Figure 3d,e, demonstrating how a field induced upshift of the HOMO level leads to ionization of the MnPc molecule. The energy diagrams without applying tip−sample bias (V_b = 0; Figure 3d) and above the charging bias V_c (Figure 3e) are given in blue and red color, respectively, and the voltage drop in the junction is shown by sloped barriers. Within the DBTJ scheme, the voltage drop occurs in two parts: in the vacuum region (between tip and molecule) and in the h-BN layer (between molecule and Rh(111) substrate). Therefore, the HOMO of MnPc raises in energy by $\Delta E = \alpha e V_b$ with respect to the Fermi energy of the Rh(111) upon increasing V_b. Once the HOMO aligns with the Fermi level of Rh(111) at V_c (when $\alpha e V_c = \Delta E_c = E_{HOMO}$), one electron is transferred and the neutral $MnPc^0$ becomes ionized to $MnPc^+$. The positive ion is characterized by a *d* orbital at lower energy (position changed from neutral (blue) to charged (red) energy level in Figure 3e). This results in a sizable jump in the tunneling current and a corresponding sharp peak in d*I*/d*V* at V_c as resonant tunneling through the *d* orbital becomes possible. Although charging peaks have been observed for other systems,[25−27,37,41,43,44,46,47] the impact on the molecular orbitals (*d* orbital in the present work) has not been studied in great detail. Within the DBTJ model in Figure 3e, the positions of HOMO (V_{HOMO}) and charging peak (V_c) in the d*I*/d*V* spectrum should be linearly correlated by $\Delta E_c = E_{HOMO}$, *i.e.*, $\alpha e V_c = (1 - \alpha) e V_{HOMO}$. As seen in the diagram of Figure 3f this is indeed the case and the linear fit gives a slope of $\alpha/(1 - \alpha) \sim 0.1$. Alternatively, α can be estimated by the relation $\alpha = d/(d + \varepsilon z)$, using the model of two parallel plate capacitors[37,38,48] where d = 0.2 nm is the thickness[28] and $\varepsilon = 4$ is the dielectric constant[49] of the h-BN layer, respectively. By estimating the distance between tip and molecule as $z \sim$ 0.5 nm, we obtain $\alpha \sim 0.09$, which agrees well with the experimental value. Because of the factor of $\alpha \sim 0.1$ and the close proximity of the HOMO to the Fermi level, a small shift in HOMO energy results in a 10 times larger change of the position of the charging peak, explaining its large variability.

Finally, we want to correlate the energetic position of the BC MnPc HOMO with the adsorption configuration. As seen from upper panel of Figure 4a, two predominant adsorption orientations for BC MnPc molecules can be observed: orientation A (marked by green lines) aligning the molecules high symmetry axis with the [12] direction of the h-BN lattice, and orientation B (marked by blue lines), where the molecule is rotated by 15° with respect to orientation A (*cf.* Figure 4c for the alignment). Note that because of the 4-fold symmetry of MnPc and the 3-fold symmetry of the h-BN/Rh(111), a rotation of 30° of MnPc with respect to h-BN/Rh(111) corresponds to the equivalent orientation. The STM topography measured at 2 V (*cf.* lower panel of Figure 4a, the blue and green lines for orientations are taken from the upper panel of Figure 4a) shows that all the molecules with orientation A are in the charged state, imaged with a "bright disk" around the molecules center,[27] while all the molecules with orientation B remain neutral and might become charged with a bias larger than 2 V. Based on the correlation between HOMO level and the required charging bias (*cf.* Figure 3f), the HOMO of molecules in orientation A should be closer to the Fermi level than that of a MnPc molecule in orientation B. This is indeed what we observe in the d*I*/d*V* spectra (*cf.* Figure 4b). Statistically, the HOMO position of the molecules with orientation A and B is −81 ± 31 mV and −173 ± 17 mV, respectively. For images taken at 2 V and 20 pA, 60 out of 71 (84%) charged MnPc are of orientation A, and 17 out of 22 (77%) neutral MnPc are of orientation B. Although the orientation does not determine the charge state exclusively, the preference is clearly seen. Exceptions might originate from the local environment, providing additional doping (impurities or defects) or the assignment of molecules just getting charged at around 2 V.

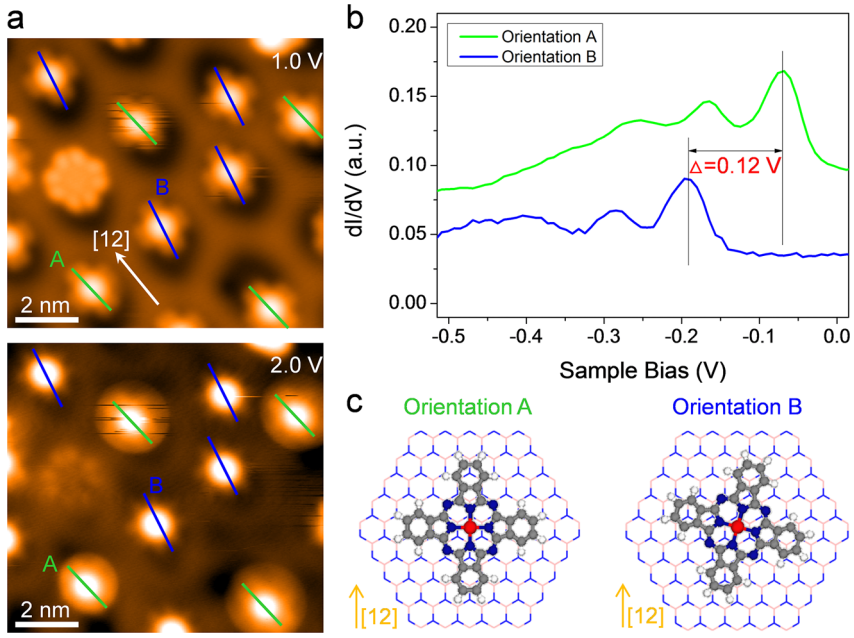

Figure 4. Adsorption orientation dependent charging. (a) STM topographic images showing the dependence of charging with adsorption orientations. Upper image taken at 1.0 V shows the orientation, while the lower image taken at 2.0 V indicates whether the molecules are charged or not. (b) d*I*/d*V* spectra demonstrate the difference in HOMO position of BC MnPc molecules with different adsorption orientations (measured at the isoindole unit, showing a shift of 0.12 V, curves are vertically displaced for better visibility). (c) Model structures of MnPc on the h-BN lattice with the adsorption orientations A and B. The pore and wire superstructure is omitted. The lateral adsorption position of the molecules is not known and just shown tentatively.

CONCLUSION

In summary we have shown that the surface of h-BN/Rh(111), which is usually considered to be inert, can have dramatic influence on the electronic properties of adsorbed MnPc molecules. Because of slight differences in the adsorption configuration, MnPc molecules are observed with three different types of STM/STS signatures, with distinct bias dependence. The BC (bright center) type shows a pronounced field-induced charge transfer characteristics. By careful analysis of the dependence of d*I*/d*V* spectra on the STM tip position (lateral displacement and vertical distance), we correlate the energy position of the HOMO with the charging voltage of the $MnPc^0 \rightarrow MnPc^+$ transition and follow the jump of the Mn 3*d*-related LUMO during this transition. These investigations show that a small shift in HOMO position, induced already by different adsorption orientations with respect to the h-BN substrate, results in large changes of the charging bias, thus can be used to tune the "on" and "off" state of the charging. Furthermore, our investigations highlight the complexity of the alignment of molecular energy levels occurring at the interface with large bandgap semiconductors and its impact on the field-induced charge transfer properties that arise already at a clean and atomically well-defined substrate. The understanding of the origin of this complexity is crucial in view of optimizing the performance of organic electronic devices, where large bandgap materials are frequently used as electrodes.

METHODS

All experiments were performed in a UHV instrument (base pressure 5×10^{-11} mbar) comprising a low-temperature scanning tunneling microscope operated at 4.9 K (LT-STM, Omicron). The rhodium single crystal (Rh(111)) was cleaned by repeated cycles of Ar^+ ion sputtering (750 eV, grazing incidence) and thermal annealing at 1200 K. The monolayer of h-BN was grown by thermal dehydrogenation of borazine ($(HBNH)_3$, ~50 Langmuir) on the hot Rh(111) surface (1100 K),[16,17,50] followed by postdeposition annealing at 1100 K for 12 min to promote uniform layer morphology. Subsequently, commercial MnPc molecules (see Figure 1a, Sigma-Aldrich, 97% purity) were sublimated from a Knudsen-type evaporator (after thorough thermal purification) with a deposition rate of approximately 0.1 ML/min, while the substrate was held at room temperature. The PtIr tips were etched and the STM images were acquired in the constant-current mode with bias voltage applied to the sample. Spectroscopic measurements were performed with a Lock-in amplifier (Zurich Instruments) at 10 mV rms sinusoidal modulation at a frequency of 610 Hz.

Conflict of Interest: The authors declare no competing financial interest.

Acknowledgment. This work was supported by the Swiss National Science Foundation (SNSF; CRSI20-122 703 and 200021_149627). O.G. and L.L. would like to thank the EU-EMPA COFUND Project BONMAT. We gratefully acknowledge H. Sachdev for providing the borazine for the h-BN growth.

Supporting Information Available: The Supporting Information is available free of charge on the ACS Publications website at DOI: 10.1021/acsnano.5b03741.

Bias dependence of the STM topography appearance of MnPc on h-BN/Rh(111). Structural integrity and purity on the adsorbed MnPc. Statistical analysis of the MnPc occurrence and orientation. High resolution STS of the HOMO for different BC charging cases. *I*(*V*) characteristics of the BC charging. 2D spatial-bias dependence of charging transition. Tip height dependence of charging peak. Correlation between orientations of the BC MnPc and charging characteristics. (PDF)

REFERENCES AND NOTES

1. Oregan, B.; Gratzel, M. A Low-Cost, High-Efficiency Solar-Cell Based on Dye-Sensitized Colloidal TiO_2 Films. *Nature* **1991**, *353*, 737–740.
2. Nelson, J. Organic Photovoltaic Films. *Curr. Opin. Solid State Mater. Sci.* **2002**, *6*, 87–95.
3. Geffroy, B.; le Roy, P.; Prat, C. Organic Light-Emitting Diode (OLED) Technology: Materials, Devices and Display Technologies. *Polym. Int.* **2006**, *55*, 572–582.
4. Schneider, J.; Matsuoka, M.; Takeuchi, M.; Zhang, J. L.; Horiuchi, Y.; Anpo, M.; Bahnemann, D. W. Understanding TiO_2 Photocatalysis: Mechanisms and Materials. *Chem. Rev.* **2014**, *114*, 9919–9986.
5. Greiner, M. T.; Helander, M. G.; Tang, W. M.; Wang, Z. B.; Qiu, J.; Lu, Z. H. Universal Energy-Level Alignment of Molecules on Metal Oxides. *Nat. Mater.* **2012**, *11*, 76–81.
6. Lu, X.; Grobis, M.; Khoo, K.; Louie, S.; Crommie, M. Charge Transfer and Screening in Individual C60 Molecules on Metal Substrates: A Scanning Tunneling Spectroscopy and Theoretical Study. *Phys. Rev. B: Condens. Matter Mater. Phys.* **2004**, *70*, 115418.
7. Wiessner, M.; Hauschild, D.; Sauer, C.; Feyer, V.; Scholl, A.; Reinert, F. Complete Determination of Molecular Orbitals by Measurement of Phase Symmetry and Electron Density. *Nat. Commun.* **2014**, *5*, 4156.
8. Gottfried, J. M. Surface Chemistry of Porphyrins and Phthalocyanines. *Surf. Sci. Rep.* **2015**, *70*, 259–379.
9. Peisert, H.; Uihlein, J.; Petraki, F.; Chassé, T. Charge Transfer between Transition Metal Phthalocyanines and Metal Substrates: The Role of the Transition Metal. *J. Electron Spectrosc. Relat. Phenom.* **2015**, DOI: 10.1016/j.elspec.2015.01.005.
10. Repp, J.; Meyer, G.; Stojković, S.; Gourdon, A.; Joachim, C. Molecules on Insulating Films: Scanning Tunneling Microscopy Imaging of Individual Molecular Orbitals. *Phys. Rev. Lett.* **2005**, *94*, 026803.
11. Heinrich, A. J.; Gupta, J. A.; Lutz, C. P.; Eigler, D. M. Single Atom Spin Flip Spectroscopy. *Science* **2004**, *306*, 466–469.
12. Hirjibehedin, C. F.; Lutz, C. P.; Heinrich, A. J. Spin Coupling in Engineered Atomic Structures. *Science* **2006**, *312*, 1021–1024.
13. Nilius, N.; Wallis, T.; Ho, W. Influence of a Heterogeneous Al_2O_3 Surface on the Electronic Properties of Single Pd Atoms. *Phys. Rev. Lett.* **2003**, *90*, 046808.
14. Dil, H.; Lobo-Checa, J.; Laskowski, R.; Blaha, P.; Berner, S.; Osterwalder, J.; Greber, T. Surface Trapping of Atoms and Molecules with Dipole Rings. *Science* **2008**, *319*, 1824–1826.
15. Cun, H.; Iannuzzi, M.; Hemmi, A.; Roth, S.; Osterwalder, J.; Greber, T. Immobilizing Individual Atoms beneath a Corrugated Single Layer of Boron Nitride. *Nano Lett.* **2013**, *13*, 2098–2103.
16. Berner, S.; Corso, M.; Widmer, R.; Groening, O.; Laskowski, R.; Blaha, P.; Schwarz, K.; Goriachko, A.; Over, H.; Gsell, S.; *et al.* Boron Nitride Nanomesh: Functionality from a Corrugated Monolayer. *Angew. Chem., Int. Ed.* **2007**, *46*, 5115–5119.
17. Widmer, R.; Passerone, D.; Mattle, T.; Sachdev, H.; Groning, O. Probing the Selectivity of a Nanostructured Surface by Xenon Adsorption. *Nanoscale* **2010**, *2*, 502–508.
18. Iannuzzi, M.; Tran, F.; Widmer, R.; Dienel, T.; Radican, K.; Ding, Y.; Hutter, J.; Groning, O. Site-Selective Adsorption of Phthalocyanine on h-BN/Rh(111) Nanomesh. *Phys. Chem. Chem. Phys.* **2014**, *16*, 12374.
19. Natterer, F. D.; Patthey, F.; Brune, H. Quantifying Residual Hydrogen Adsorption in Low Temperature STMs. *Surf. Sci.* **2013**, *615*, 80–87.
20. Zhang, J.; Sessi, V.; Michaelis, C. H.; Brihuega, I.; Honolka, J.; Kern, K.; Skomski, R.; Chen, X.; Rojas, G.; Enders, A. Ordered Layers of Co Clusters on BN Template Layers. *Phys. Rev. B: Condens. Matter Mater. Phys.* **2008**, *78*, 165430.
21. Schulz, F.; Drost, R.; Hamalainen, S. K.; Liljeroth, P. Templated Self-Assembly and Local Doping of Molecules on Epitaxial Hexagonal Boron Nitride. *ACS Nano* **2013**, *7*, 11121–11128.
22. Joshi, S.; Bischoff, F.; Koitz, R.; Ecija, D.; Seufert, K.; Seitsonen, A. P.; Hutter, J.; Diller, K.; Urgel, J. I.; Sachdev, H.; *et al.* Control of Molecular Organization and Energy Level Alignment by an Electronically Nanopatterned Boron Nitride Template. *ACS Nano* **2014**, *8*, 430–442.
23. Dienel, T.; Gomez-Diaz, J.; Seitsonen, A. P.; Widmer, R.; Iannuzzi, M.; Radican, K.; Sachdev, H.; Mullen, K.; Hutter, J.; Groning, O. Dehalogenation and Coupling of a Polycyclic Hydrocarbon on an Atomically Thin Insulator. *ACS Nano* **2014**, *8*, 6571–6579.
24. Schulz, F.; Ijas, M.; Drost, R.; Hamalainen, S. K.; Harju, A.; Seitsonen, A. P.; Liljeroth, P. Many-Body Transitions in a Single Molecule Visualized by Scanning Tunnelling Microscopy. *Nat. Phys.* **2015**, *11*, 229–234.
25. Pradhan, N. A.; Liu, N.; Silien, C.; Ho, W. Atomic Scale Conductance Induced by Single Impurity Charging. *Phys. Rev. Lett.* **2005**, *94*, 076801.
26. Teichmann, K.; Wenderoth, M.; Loth, S.; Ulbrich, R. G.; Garleff, J. K.; Wijnheijmer, A. P.; Koenraad, P. M. Controlled Charge Switching on a Single Donor with a Scanning Tunneling Microscope. *Phys. Rev. Lett.* **2008**, *101*, 076103.
27. Cui, Y.; Nilius, N.; Freund, H.-J.; Prada, S.; Giordano, L.; Pacchioni, G. Controlling the Charge State of Single Mo Dopants in a CaO Film. *Phys. Rev. B: Condens. Matter Mater. Phys.* **2013**, *88*, 205421.
28. Laskowski, R.; Blaha, P.; Gallauner, T.; Schwarz, K. Single Layer Model of the Hexagonal Boron Nitride Nanomesh on the Rh(111) Surface. *Phys. Rev. Lett.* **2007**, *98*, 106802.
29. Bartels, L.; Meyer, G.; Rieder, K. H. Basic Steps of Lateral Manipulation of Single Atoms and Diatomic Clusters with a Scanning Tunneling Microscope Tip. *Phys. Rev. Lett.* **1997**, *79*, 697.
30. Liu, L.; Yang, K.; Jiang, Y.; Song, B.; Xiao, W.; Li, L.; Zhou, H.; Wang, Y.; Du, S.; Ouyang, M.; *et al.* Reversible Single Spin Control of Individual Magnetic Molecule by Hydrogen Atom Adsorption. *Sci. Rep.* **2013**, *3*, 1210.
31. Stróżecka, A.; Soriano, M.; Pascual, J. I.; Palacios, J. J. Reversible Change of the Spin State in a Manganese Phthalocyanine by Coordination of CO Molecule. *Phys. Rev. Lett.* **2012**, *109*, 147202.
32. Yang, K.; Liu, L. W.; Zhang, L. Z.; Xiao, W. D.; Fei, X. M.; Chen, H.; Du, S. X.; Ernst, K. H.; Goo, H. J. Reversible Achiral-to-Chiral Switching of Single Mn-Phthalocyanine Molecules by Thermal Hydrogenation and Inelastic Electron Tunneling Dehydrogenation. *ACS Nano* **2014**, *8*, 2246–2251.
33. Ge, X.; Manzano, C.; Berndt, R.; Anger, L. T.; Kohler, F.; Herges, R. Controlled Formation of an Axially Bonded Co-Phthalocyanine Dimer. *J. Am. Chem. Soc.* **2009**, *131*, 6096–6098.
34. For the peak intensity distribution and HOMO position at the lobe and at the center, Please refer to Supporting Information: High resolution STS of the HOMO for different BC charging cases.
35. Matino, F.; Schull, G.; Kohler, F.; Gabutti, S.; Mayor, M.; Berndt, R. Electronic Decoupling of a Cyclophane from a Metal Surface. *Proc. Natl. Acad. Sci. U. S. A.* **2011**, *108*, 961–964.
36. Qiu, X. H.; Nazin, G. V.; Ho, W. Vibronic States in Single Molecule Electron Transport. *Phys. Rev. Lett.* **2004**, *92*, 206102.
37. Fernández-Torrente, I.; Kreikemeyer-Lorenzo, D.; Stróżecka, A.; Franke, K. J.; Pascual, J. I. Gating the Charge State of Single Molecules by Local Electric Fields. *Phys. Rev. Lett.* **2012**, *108*, 036801.

38. Hauptmann, N.; Hamann, C.; Tang, H.; Berndt, R. Switching and Charging of a Ruthenium Dye on Ag(111). *Phys. Chem. Chem. Phys.* **2013**, *15*, 10326–10330.
39. Preuss, M.; Bechstedt, F. Vibrational Spectra of Ammonia, Benzene, and Benzene Adsorbed on Si(001) by First Principles Calculations with Periodic Boundary Conditions. *Phys. Rev. B: Condens. Matter Mater. Phys.* **2006**, *73*, 155413.
40. Sauvage, F. X.; Debacker, M. G.; Stymne, B. An Infrared Study of the Complexing Ability of Manganese Phthalocyanine. *Spectrochim. Acta. A* **1982**, *38*, 281–288.
41. Nazin, G. V.; Qiu, X. H.; Ho, W. Charging and Interaction of Individual Impurities in a Monolayer Organic Crystal. *Phys. Rev. Lett.* **2005**, *95*, 166103.
42. Warner, B.; El Hallak, F.; Pruser, H.; Sharp, J.; Persson, M.; Fisher, A. J.; Hirjibehedin, C. F. Tunable Magnetoresistance in an Asymmetrically Coupled Single-Molecule Junction. *Nat. Nanotechnol.* **2015**, *10*, 259–263.
43. Zheng, H.; Weismann, A.; Berndt, R. Manipulation of Subsurface Donors in ZnO. *Phys. Rev. Lett.* **2013**, *110*, 226101.
44. Brar, V. W.; Decker, R.; Solowan, H. M.; Wang, Y.; Maserati, L.; Chan, K. T.; Lee, H.; Girit, C. O.; Zettl, A.; Louie, S. G.; *et al.* Gate Controlled Ionization and Screening of Cobalt Adatoms on a Graphene Surface. *Nat. Phys.* **2011**, *7*, 43–47.
45. Tunneling parameter before opening FB loop: 2 V, 200 pA for the charging peak, and −0.1 V, 100 pA for the HOMO. Note that the charging peak positon is highly tip height dependent, while the HOMO energy is almost tip height independent.
46. Song, C.-L.; Jiang, Y.-P.; Wang, Y.-L.; Li, Z.; Wang, L.; He, K.; Chen, X.; Ma, X.-C.; Xue, Q.-K. Gating the Charge State of Single Fe Dopants in the Topological Insulator Bi_2Se_3 with a Scanning Tunneling Microscope. *Phys. Rev. B: Condens. Matter Mater. Phys.* **2012**, *86*, 045441.
47. Zheng, H.; Weismann, A.; Berndt, R. Tuning the Electron Transport at Single Donors in Zinc Oxide with a Scanning Tunnelling Microscope. *Nat. Commun.* **2014**, *5*, 2992.
48. Nazin, G. V.; Wu, S. W.; Ho, W. Tunneling Rates in Electron Transport through Double Barrier Molecular Junctions in a Scanning Tunneling Microscope. *Proc. Natl. Acad. Sci. U. S. A.* **2005**, *102*, 8832–8837.
49. Arya, S. P. S.; Damico, A. Preparation, Properties and Applications of Boron-Nitride Thin-Films. *Thin Solid Films* **1988**, *157*, 267–282.
50. Muller, F.; Hufner, S.; Sachdev, H. Epitaxial Growth of Boron Nitride on a Rh(111) Multilayer System: Formation and Fine Tuning of a BN-Nanomesh. *Surf. Sci.* **2009**, *603*, 425–432.